Friction Dynamics Simulation Analysis Of Stirling Engine Piston Ring

Mingru Lei[1], Haiyong Peng[1*], Yuchen Jiang[1], Yi Cui[2*], and Yun Guo[1]

[1] School of Mechanical and Automotive Engineering, Shanghai University of Engineering Science, Shanghai 201600, China
[2] School of Mechanical Engineering, Shanghai Jiao Tong University, Shanghai 201100, China
[*] Corresponding author. E-mail: penghy@sues.edu.cn, ycui@sjtu.edu.cn

Received: Oct. 9, 2025; Accepted: Feb. 07, 2026

The reliability and durability of piston rings in double-acting Stirling engines are critical to overall engine performance. This study investigates the dynamic tribological behavior of the piston ring-cylinder liner contacts during operation. By establishing a coupled dynamic-tribological-leakage simulation model, the friction, sealing, and wear performance of the ring pack under rated and variable-speed operating conditions are systematically analyzed. Under the rated condition of 1800r/min, the instantaneous maximum friction forces of the top ring and the second ring are 392.3 N and 163.7 N, respectively, while the corresponding cycle-averaged friction forces are 147.9 N and 94.8 N. The instantaneous peak frictional power losses are 1360 W and 590 W, and the cycle-averaged frictional power losses are 470.2 W and 309.3 W, respectively. The peak total contact pressures reach 18.9 MPa for the top ring and 13.55 MPa for the second ring, and the maximum radial wear depths after 100 h of operation are 0.121 mm and 0.115 mm, respectively. When the rotational speed increases from 900r/min to 3600 r/min, the blow-by of the ring pack decreases by 68.8%, whereas the total frictional power loss and the wear rate increase by 229% and 122%, respectively. These results quantitatively reveal an inherent and previously unresolved trade-off between sealing performance and wear life for filled PTFE composite piston rings in double-acting Stirling engines. The proposed framework provides physically based design metrics for ring material selection, ring geometry optimization, and operating-condition assessment, and supports reliable sealing performance and service-life prediction for Stirling engine applications.

Keywords: dynamic simulation; oil-free lubrication seal; sealing performance; Blow-by

http://dx.doi.org/10.6180/jase.202609_32.004

1. Introduction

The Stirling engine is a closed-cycle power device with considerable application potential, particularly in applications requiring flexible heat sources, high thermal efficiency, and low emissions [1–3]. Increasing the working pressure is an effective approach to achieving higher power density and output power in Stirling engine systems [4, 5]; however, higher pressures impose more stringent requirements on the dynamic sealing performance and oil-free lubrication of the piston ring pack [6]. For double-acting Stirling engines, in which the piston separates two working fluid chambers, reliable sealing is essential, as working gas leakage (blow-by) and ring wear directly reduce efficiency and shorten service life.

During the operation of double-acting Stirling engines, piston rings are subjected to severe and strongly coupled challenges, including alternating loads, high temperature and pressure, oil-free sliding conditions, and interactions among ring dynamics, asperity contact on rough surfaces, and gas flow through ring gaps. Polytetrafluoroethylene (PTFE)-based composite materials are commonly selected as ring materials because of their self-lubricating properties and temperature resistance [7, 8], and their tribological performance critically depends on transfer film formation, filler content, and contact pressure distribution [9, 10]. Previous experimental and theoretical studies have character-

ized PTFE transfer films and wear mechanisms (fatigue wear and abrasive wear) [11–13], and have provided empirical wear correlations for PTFE-metal friction pairs [14–16]. However, these studies mainly offer qualitative or empirical descriptions of the wear behavior of filled PTFE materials and do not provide quantitative comparisons of wear performance for filled PTFE-metal friction pairs.

In addition, advances in numerical modeling of Stirling engines have promoted the development of thermodynamic-dynamic coupled simulations [17–20]. Although these studies provide predictions of overall engine dynamics, piston sealing behavior is usually treated using simplified assumptions, and friction, blow-by, and wear are not explicitly resolved at the piston ring scale. Meanwhile, other studies have focused on the tribological behavior and wear mechanisms of PTFE-based piston rings under oilfree lubrication conditions in Stirling engines [21–23]. These studies rely on averaged contact conditions and do not consider the time-varying contact pressure or ring dynamics within an operating cycle. Investigations into leakage characteristics in reciprocating seals have shown that nonuniform pressure distributions and annular gap geometries strongly influence leakage flow and local contact loads [24, 25]. However, in these studies, leakage evaluation is generally not synchronously coupled with friction dynamics or progressive wear, and therefore cannot capture the mutual feedback among these processes.

The Archard adhesive wear model [26] and its extended forms [27, 28] are still widely used in engineering applications. Based on Archard wear theory, Ding et al. [29] and Békési et al. [30] incorporated pressure-induced load variations or fracture criteria into wear life analysis, while Cao et al. [31] introduced dynamic mesh updating to simulate geometry evolution under wear. Despite these advances, wear prediction is typically decoupled from transient blow-by and ring dynamics, and most models assume steady or cycle-averaged loading conditions.

By contrast, in the field of internal combustion engines, Razavirad et al. [32] achieved synchronous wear calculation of piston rings and cylinder liners under dry friction conditions. Ahmed Ali et al. [33] established a coupled piston ring dynamics and mixed lubrication model based on the Reynolds equation and the Greenwood-Tripp rough surface contact model, while Mahmoud et al. [34] and Mahmoud et al. [35] developed three-dimensional ring pack models incorporating liner deformation, inter-ring gas flow, and lubrication effects. These studies clearly demonstrate that ring dynamics, gas flow, and contact mechanics must be treated within an integrated framework. However, they were developed for metallic ring-liner systems in internal combustion engines, and their assumptions and conclusions cannot be directly applied to oil-free PTFE composite rings.

In summary, existing studies have largely addressed PTFE composite tribology, engine dynamics, blow-by, and wear prediction in a decoupled manner. For example, some models predict wear [21, 29], while others analyze gas flow or friction [22, 25]. To date, no published work has simultaneously integrated friction dynamics, blow-by, and quantitative wear prediction for filled PTFE composite piston rings in double-acting Stirling engines. In such engines, the piston ring separates two pressurized working chambers, making the coupling mechanisms among ring motion, leakage, and wear fundamentally different from those in conventional single-acting or lubricated systems.

A fully coupled dynamic-tribological-leakage framework is therefore required; however, the absence of such a framework has limited the reliable prediction of sealing performance and service life for Stirling engines operating under oil-free and highpressure conditions. To address these limitations, this study proposes, for the first time, a fully coupled dynamic-tribological-leakage simulation framework for filled PTFE composite piston rings in a double-acting Stirling engine. The interactions among these mechanisms under oil-free, high-pressure operating conditions are comprehensively investigated, the dynamic tribological behavior and sealing characteristics under rated operation are quantitatively evaluated, and the influence of rotational speed is rigorously assessed.

2. Materials and methods

2.1. Theoretical analysis

Based on the actual operating conditions of the prototype used in this study, the piston ring sealing arrangement and the forces acting on a single ring in the Stirling engine are shown in Fig. 1.

Here, p_1 denotes the hot-chamber pressure and p_2 the cold-chamber pressure; the top ring is referred to as Ring 1 and the second ring as Ring 2. Both sealing rings are open-ended (split) rings with straight cuts, and the guide ring is fitted with pressurerelief holes.

During engine operation, and in accordance with Hooke's law, the tensile stress σ experienced by the ring may be expressed as follows [36]:

$$\sigma = E\varepsilon = E\frac{\delta}{R_0} = E\frac{R - R_0}{R_0} \tag{1}$$

Where E is the Young's modulus of the piston ring material under operating conditions (MPa); R is the ring's mean radius during operation (mm); R_0 is the ring's mean

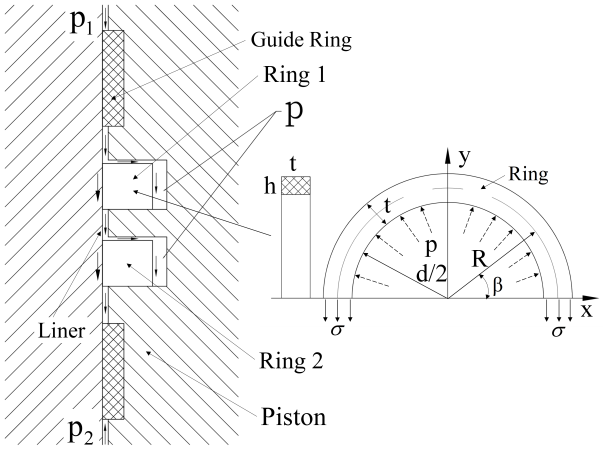

Fig. 1. Schematic of the piston ring pack configuration and ring stress distribution [36]

radius at ambient (room) temperature (mm); and $\underline{\varepsilon}$ is the radial tensile elastic deformation of the ring caused by the temperature rise during operation (mm).

From the mechanical equilibrium it follows that the resultant of the tensile stress σ over the cross-section in the y-direction is equal to the y-component of the force produced by the back-pressure p acting on the inner side of the ring, Its formula is as follows [37]:

$$2ht\sigma = \int_0^{\pi} \left(phd \sin \frac{\beta}{2} \right) d\beta = phd_j \tag{2}$$

By substituting Eq. (1) into Eq. (2), the formula for calculating the ring back-pressure p is obtained:

$$p = \frac{2Et\,(R - R_0)}{dR_0} \tag{3}$$

Eq. (4) is used to calculate the piston ring's mean radius after the temperature rise [37]:

$$R = R_0(1 + \alpha \Delta T) \tag{4}$$

Substituting Eq. (4) into Eq. (3) yields the expression relating the ring back pressure p to the operating temperature:

$$p = \frac{2Et\alpha\,(T_1 - T_0)}{d} \tag{5}$$

The static friction force of the ring pack, when it establishes a static seal in the ring groove, is given by Eq. (6) [22]:

$$\begin{aligned} F_f &= \mu \left[\frac{2Et\alpha\,(T_1 - T_0)}{d} + \frac{EA_e}{3.54D(D/t - 1)} - 0.96P_1 \right] \\ &= F_f\,(T_1, P_1) \end{aligned} \tag{6}$$

Where :

F_f : the static friction force of the piston ring in the static sealing state (N); P_1: the pressure of the sealing medium (gas) (MPa); T_1: the operating temperature (°C); T_0: the initial temperature (°C) ; D : the outer diameter of the piston ring (mm); t : the ring's radial width (mm); h: the ring's axial thickness (mm); d: the inner diameter of the ring (mm); A_e: the size of the straight cut opening (mm); α : the linear thermal expansion coefficient of the ring material ($°C^{-1}$).

The piston ring surface and the cylinder wall undergo relative sliding, producing sliding friction on the sealing surface. The magnitude of this sliding friction depends on the relative velocity between the contacting bodies; hence, the piston velocity directly influences the sliding friction. Under sealed conditions, the sliding frictional force F_d is given by [22]:

$$F_d = F_f\,(T_1, P_1) + k_1 v^2 - k_2 v = F_d\,(T_1, P_1, v) \tag{7}$$

According to the peeling-wear theory [38], the radial wear volume Q_1 can be calculated using Eq. (8); this volume is obtained from the temperature variation associated with the relative sliding of the ring [23]:

$$Q_1 = K_S pSL \tag{8}$$

Where S denotes the sliding distance (mm), L is the contact area between the ring and the liner $(L = ht)$ (mm^2), and K_s is the wear modulus $(\mathrm{mm}^3/\mathrm{Nm})$, v : Poisson's ratio (-).

In summary, the variation of piston-ring radial wear volume with temperature can be expressed by Eq. (9):

$$Q_1 = K_S SL \frac{2Et}{d} \alpha\,(T_1 - T_0) \tag{9}$$

2.2. Model assumptions and simplifications

For a double-acting Stirling engine, inter-cylinder pressure coupling may induce gas "pumping" effects that influence local pressure fluctuations and leakage behavior. To simplify the analysis, this study neglects inter-cylinder "pumping" and focuses on a single-cylinder equivalent model of the piston ring-liner sealing system. Based on published studies on double-acting Stirling engines and oil-free reciprocating sealing systems [25, 29], the omission of inter-cylinder gas pumping typically results in an underestimation of blow-by on the order of $5 - 15\%$, depending on phase angle and pressure coupling intensity. However, this simplification does not affect the comparative trend analysis with rotational speed, which is the primary focus of this study.

Furthermore, the following assumptions are also adopted:

(1) Wear of the piston ring is assumed to occur predominantly in the radial direction. Axial wear is neglected,

as previous studies indicate that axial wear has a much weaker impact on sealing clearance compared to radial wear [39].

(2) Leakage caused by early structural failure, fracture, or abnormal deformation of the piston ring is not considered.

(3) The sealing components between the piston and the cylinder comprise the guide rings and the piston rings, as shown in Fig. 1. The guide rings are equipped with pressure relief holes and do not serve a sealing function; thus, they are assumed to have no effect on the sealing performance of the piston ring pack.

(4) Wear mechanisms in oil-free piston rings are complex, with comparatively consistent and predictable behavior observed solely in the stable wear phase. Therefore, this study concerns itself solely with the steady wear phase occurring during normal operation.

(5) This study focuses on the influence of macroscopic piston-ring wear on the sealing performance, service life, and lubrication of the piston ring-cylinder sealing system, and does not consider changes in the ring's material properties during the wear process. Experimental studies indicate that, after entering the steady wear stage, the mechanical properties of filled PTFE composites exhibit minimal temporal variation [14, 38].

(6) Young's modulus of the piston ring material is treated as constant within the operating temperature range considered in this study (approximately $80 - 120°C$). Experimental data for similar glass-fiber reinforced PTFE materials show that the variation in Young's modulus within this range is typically within $\pm 10\%$ [13, 40]. Given that Young's modulus mainly affects thermal expansion-related restoring forces, this assumption has a limited influence on friction, contact pressure, and wear trends, which are primarily governed by pressure boundary conditions and surface contact mechanics.

Since the structural and motion characteristics of the Stirling engine piston ring are similar to those of internal combustion engines, this study adopts the well established dynamic simulation methods developed for internal combustion engine piston rings. After appropriate simplification of the piston ring pack-liner structure of the Stirling engine prototype, a lubrication performance analysis model of the piston ring-cylinder liner system was developed using AVL-EXCITE Piston & Rings. The model employs a two-ring configuration, both being straight-cut, open-ended rings with an end gap of 1.24 mm.

2.3. Model development

Numerical simulations were performed using AVL-EXCITE Piston & Rings [software version: R2023.1]. The solver settings and numerical parameters are listed in this Section. The calculations were executed on a workstation with: CPU = Intel Core Ultra 9185 H, number of cores = 16, RAM = 64 GB, operating system = Windows 10 x64.

The basic input parameters for the simulation model are listed in Table 1. The end gaps of the two rings are installed in the ring groove with a 180° offset. Fig. 2 presents the running surface profile of the piston ring and its installation location within the ring groove. The ring has a barrel-shaped profile. Under the rated operating conditions, the pressures in the expansion space (hot chamber) and the compression space (cold chamber) are shown in Fig. 3, with the crankcase pressure maintained constant at 10.3 MPa. The pressure boundary condition is derived from measured data, processed through interpolation and smoothing before being input into the model. The working fluid used for lubrication is helium, and its parameters were set according to the physical properties of helium. The piston ring material is glass-fiber and ferric-oxide filled PTFE. For glass-fiber-reinforced PTFE composites sliding against metallic liners under oil-free or dry-running conditions, based on experimental studies [13, 29, 40] and considering the specific material characteristics (PTFE filled with glass-fibers and ironoxide), the operating temperature (approximately 100°C), and the contact pressure levels in the present study, a wear coefficient of 1.5×10^{-6} mm^3/Nm was adopted as a representative value corresponding to steady-state wear conditions, which is capable of capturing the dominant wear behavior and trend characteristics of the piston ringcylinder liner system. In this model, the calculation step size is set to 0.1°CA. The time integration employs an implicit matrix formulation with dual convergence criteria (force and displacement iterations) at a tolerance of 1×10^{-6}. Numerical simulations were performed using AVL-EXCITE Piston & Rings, which employs a parametric reduced order discretization rather than conventional three-dimensional finite-element meshing. In the present model, the piston ring running surface was discretized circumferentially into 120 nodes, while the cylinder liner contact surface was discretized into 100 nodes for contact pressure and wear evaluation. The axial contact resolution is implicitly defined by the ring profile and groove geometry following the standard formulation of the software. The adopted discretization was verified to provide numerically stable distributions of friction force, contact pressure, and wear depth, and further refinement did not affect the qualitative trends of the results.

Table 1. Basic parameters of the piston ring-cylinder liner model

Engine parameters	Values
Rated speed (r/min)	1800
Stroke (mm)	50
Connecting rod length (mm)	140
Crank radius (mm)	25
Cylinder bore (mm)	90
Heat power (kW)	173
Clearance (μm)	50
Average operating temperature of the piston ring (°C)	100
Piston outer diameter (mm)	89.7
Cylinder liner surface roughness Ra(μm)	0.04
Piston ring surface roughness Ra(μm)	1.5
Elastic modulus of the cylinder liner (GPa)	190
Working fluid (-)	Helium
Piston ring material properties	**Values**
Density (g/cm^3)	2.645
Brinell hardness (HB)	45
Tensile strength (MPa)	20.2
Elongation at break (%)	340
Elastic modulus (MPa)	1185
Thermal expansion coefficient (1/°C)	1.22×10^{-4}
Friction coefficient (-)	0.22
Wear coefficient (mm^3/Nm)[29]	1.5×10^{-6}
Poisson's ratio (-)	0.45
Thermal conductivity W/(m · K)	0.32

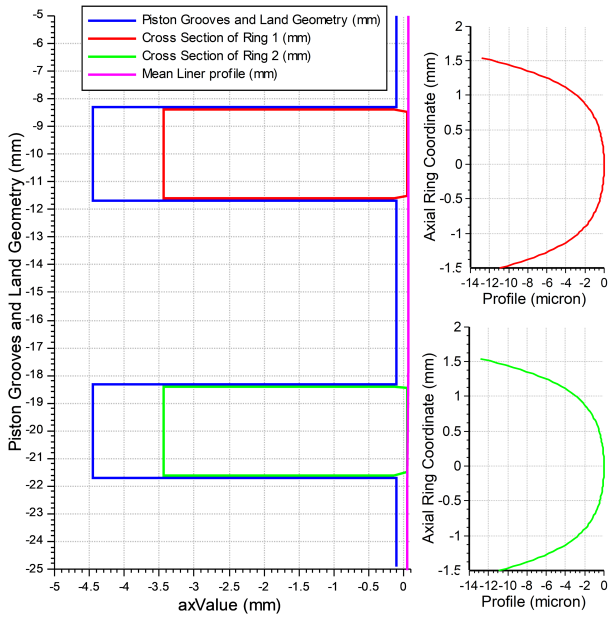

Fig. 2. Installation position and running surface profile of the piston ring

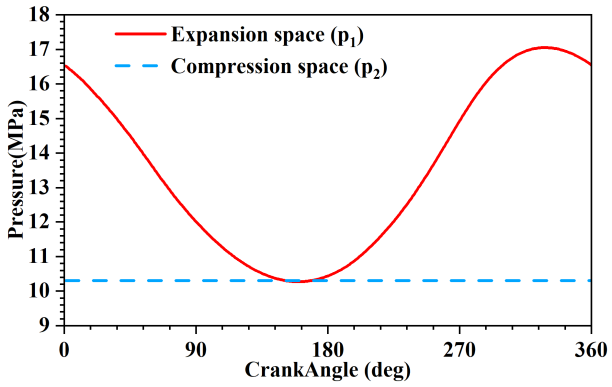

Fig. 3. Variation of expansion chamber and compression chamber pressures with crank angle

Parameter setting of the cylinder liner profile: The liner surface profile can be defined using one or more individual patches, in which the radial deviations from the reference diameter are specified. The defined patch profile of the liner is shown in Fig. 4a, and the defined liner profile is shown in Fig. 4b.

2.3.1. Motion model

The external forces applied to a single ring are illustrated in Figure 5. These forces and moments arise from gas pressure, inertial effects, ring twist and tilt, and the interactions between the piston ring groove and the liner.

Axial motion of the piston ring: When the ring is in contact with the groove side surface, the contact force be-

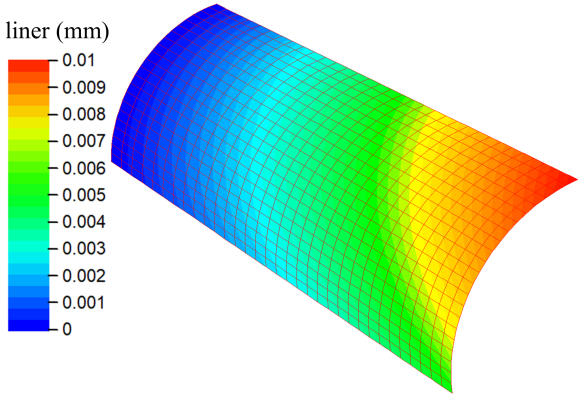

(a) Defined piston patch profile

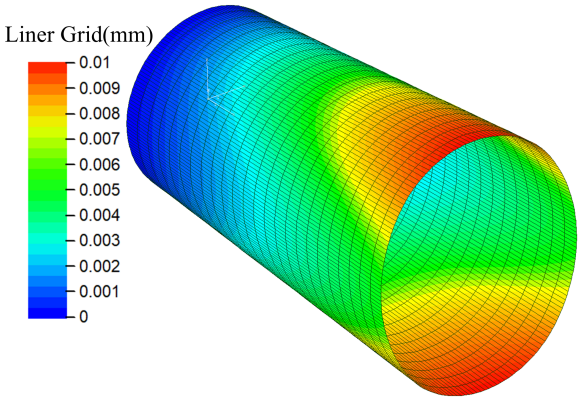

(b) Defined piston profile

Fig. 4. Definition of the cylinder liner profile

tween the ring and the groove can be obtained from the force equilibrium, as expressed by Eq. (10):

$$F_{\text{contact},ax} = F_{\text{bending}} + F_{\text{inertia},ax} + F_{\text{fric},ax} + F_{\text{gas},ax} \quad (10)$$

Where:

$F_{\text{gas},ax}$: the gas force (N); $F_{\text{inertia},ax}$: the inertia force (N); $F_{\text{fric},ax}$: the friction force between the cylinder wall and ring running surface (N); F_{bending} : the bending force caused by the interaction between the thrust and anti-thrust sides (N).

Radial motion of the piston ring: The contact force between the ring running surface and the cylinder liner is given by Eq. (11):

$$F_{\text{contact,rad}} = F_{\text{gas,rad}} + F_{\text{tension}} + F_{\text{fric,rad}} \quad (11)$$

2.3.2. *Rough contact model*

When glass fiber filled PTFE contains a relatively high filler fraction, its elastic modulus increases markedly, and under light-to-moderate loads it exhibits predominantly elastic deformation [40, 42, 43]. The statistical formulation of the Greenwood-Tripp model is appropriate for predicting

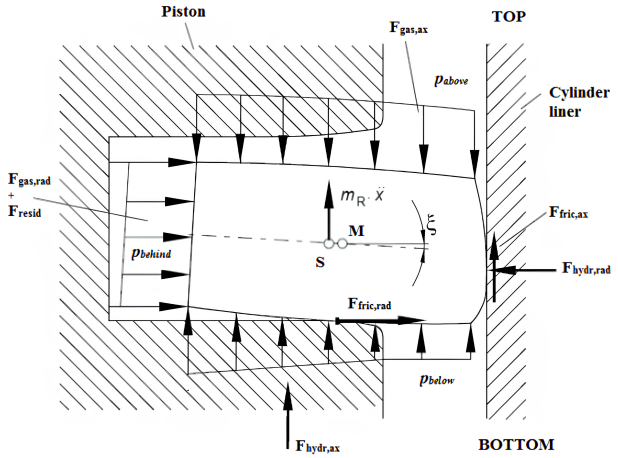

Fig. 5. Force system acting on the piston ring [41]

asperity contact density and contact-area distribution at filled PTFE metal interfaces [44]. Under light load, low interference PTFE metal contact conditions, the contact-pressure error for spherical asperities remains within a reasonable range, so the Greenwood-Tripp model's elastic assumption is still justified [45].

In this study, the piston-ring material contains a relatively high proportion of glassfiber filler, and the rings operate normally under light loads. Therefore, the rough contact process is defined here by the Greenwood-Tripp model for dry contact between rough surfaces, with the mean rough contact pressure given by the following expression [46]:

$$p_a = \frac{16\sqrt{2}\pi}{15}\left(\sigma_s \tilde{\beta}_s\right)^2 \sqrt{\frac{\sigma_s}{\beta}} E^* F_{5/2}\left(H_s\right) \quad (12)$$

Where:

$$F_{5/2} = \text{the form function} = \begin{cases} 4.4086 \times 10^{-5}\left(4 - H_s\right)^{6.804} & H_s < 4 \\ 0 & H_s \geq 4 \end{cases}$$

$$E^* = \text{composite elastic modulus} = \frac{1}{\left(\frac{1-v_1^2}{E_1} + \frac{1-v_2^2}{E_2}\right)}$$

E : Young's modulus of material near the surface (MPa); H_s: Nominal clearance between the contacting surfaces (mm); $\tilde{\beta}$: Asperity mean summit radius (μm); η_s: Number of summits in the nominal area $A(-)$; v : Poisson's ratio $(-)$; σ_s : R.M.S surface roughness (μm).

2.3.3. *Wear model*

The piston rings in the Stirling engine are made of filled PTFE and undergo relative sliding against a metal cylinder liner; their primary wear mechanism is adhesive wear. According to Archard's adhesive wear model, the wear can

be expressed as follows [26]:

$$V = \frac{KFS}{H} \tag{13}$$

Considering that the wear of the ring is mainly concentrated along the radial depth direction, both sides of Eq. (13) are divided by the wear area ΔA, yielding the following wear equation [26]:

$$h_{\text{wear}} = \frac{K}{H} PS \tag{14}$$

The wear modulus K_s is defined as $K_s = K/H\ (\mathrm{N/mm^2})$, By introducing a time interval Δt, Equation (14) can be rewritten as [26]:

$$\Delta h = K_s p_t v_r \Delta t \tag{15}$$

Where:
V : the wear volume $(\mathrm{mm^3})$; K : the dimensionless wear coefficient $(-)$; F : the normal load applied to the contact surfaces (N); S : the sliding distance (mm); H : the Brinell hardness of the softer contacting material $(\mathrm{N/mm^2})$; h: the wear depth (mm); P: the local normal pressure acting on the wear area $\Delta A(\mathrm{MPa})$; Δh: the increment of wear depth (mm); p_t: the pressure as a function of time (MPa); v_r : the relative sliding velocity $(\mathrm{mm/s})$.

3. Results and discussion

3.1. Friction force and power loss of the piston rings

Fig. 6 shows the friction force and power loss of the ring. Figs. 6a and 6b show the variation of the friction force and friction power loss between the ring and the cylinder liner with the crankshaft angle when the crankshaft speed is 1800r/min at the rated working condition. As shown in Figs. 6a and 6b, the friction force peaks between Rings 1 and 2 and the cylinder liner both occur at top dead center (TDC), with peak values of 392.3 N and 163.7 N, respectively. The corresponding peak frictional power losses are 1360 W and 590 W, which appear in the first half of the expansion stroke after TDC, indicating a clear phase lag between friction force and frictional power loss. Over a complete operating cycle, the cycle-averaged friction forces are 147.9 N and 94.8 N, respectively, while the cycle-averaged frictional power losses are 470.2 W and 309.3 W.

At TDC, the combined effects of high hot-chamber pressure, large pressure differential between the two chambers, increased ring back pressure, and thermally induced ring expansion result in the maximum normal load and thus the peak friction force. However, because the piston sliding velocity approaches zero at TDC, the instantaneous frictional power loss decreases to 0 W. After TDC, the piston velocity increases rapidly, while the rings still sustain a relatively high pressure differential [47], causing the frictional power loss to reach its maximum at a later stage of the expansion stroke. In addition, transfer-film behavior also contributes to this phase-lag phenomenon. During the early expansion stroke, the piston ring operates closer to the hot end and immediately after the reversal of motion direction, where the formation conditions of the transfer film are less favorable and its stability and effectiveness are relatively low. This condition can temporarily increase the effective friction coefficient, further enhancing the frictional power loss within this crank-angle range. These findings collectively indicate that the phase difference between the peak friction force and the peak frictional power loss reflects the coupled effects of pressure-driven loading, piston kinematics, and transient transfer-film behavior during the dynamic sealing process, while also revealing the transient characteristics of frictional energy dissipation in the piston ring-liner tribological system. Figs. 6c to 6e respectively show the effect of rotational speed on the total friction force between the ring pack and the liner, the total frictional power loss, and the radial force on the second ring caused by back pressure. Figs. 6c and 6d indicate that, during the latter phase of the compression stroke, the higher speed of 3600r/min reduces the total friction force compared with the lower speeds of 900r/min and 1800r/min. This reduction is mainly because, with the cold chamber pressure held at 10.3 MPa, the second ring carries most of the pressure differential and the back pressure on the second ring is markedly lower at high speed, which in turn reduces the radial load and the total friction force. In the remaining crank-angle ranges, changes in speed have little effect on the instantaneous total friction, since a relatively uniform transfer film forms between the rings and the liner within the normal operating-speed range. Consequently, the cycle-averaged friction forces show only minimal variation with speed, remaining within $\pm 2\%$.However, speed significantly influences the rings' fatigue life and wear life, which are jointly determined by the ring material properties and the interaction of the mating surfaces.

As shown in Fig. 6e, at 900r/min, 1800r/min and 3600r/min, the maximum total friction power loss of the ring pack in the first half of the expansion stroke is 940 W, 1850 W and 3650 W, respectively. When the speed rises from 900r/min to 3600 r/min, the maximum total friction power loss increases by about 288%. The cycleaveraged total friction power loss also increases with speed, rising from 410 W to 1349 W, an increase of about 229%.

Fig. 7 shows the frictional dynamic characteristics of the ring-liner system. Figs. 7a and 7b present, respectively, the total contact pressure and the rough contact pressure

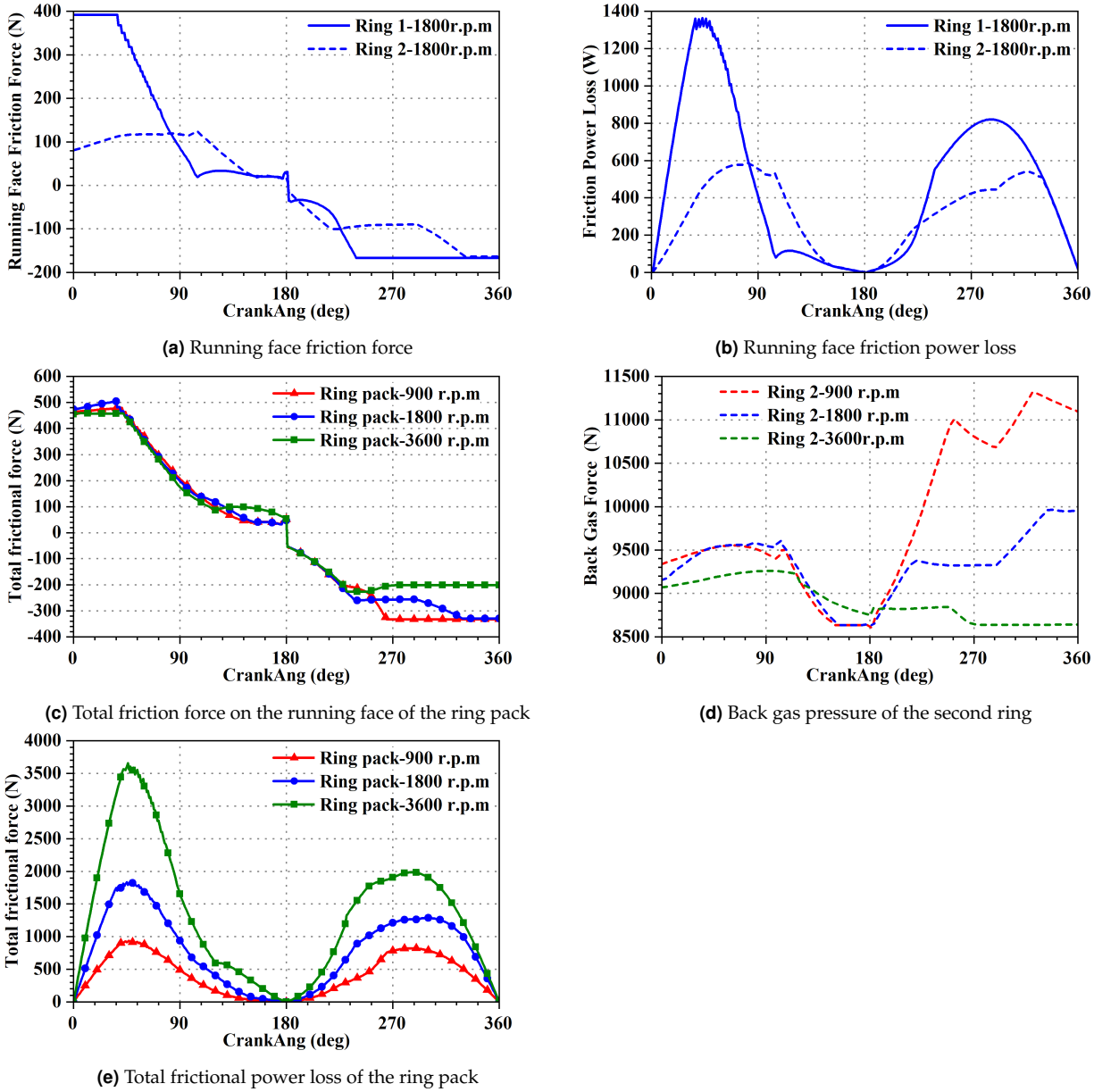

(a) Running face friction force

(b) Running face friction power loss

(c) Total friction force on the running face of the ring pack

(d) Back gas pressure of the second ring

(e) Total frictional power loss of the ring pack

Fig. 6. Friction force and power loss of the rings

between the rings and the liner; Fig. 7c show the ring pack blow-by and the effect of rotational speed on blow-by, respectively.

At the rated condition (1800r/min), Fig. 7a shows that the total contact pressure of the top ring fluctuates widely, peaking at about 18.9 MPa near the TDC of the expansion stroke and falling to roughly 1.3 MPa near the bottom dead center (BDC). The second ring's total contact pressure is relatively stable, ranging from 10.25 to 13.55 MPa, with its maximum and minimum occurring near the compression-stroke TDC and BDC, respectively. These differences indicate that the top ring plays the dominant role in instantaneous sealing and load carrying, while the second ring mainly provides auxiliary sealing. Fig. 7b shows that the rough-contact pressure exhibits the same crank-angle dependence as the normal load: its maximum value of 2.075 MPa occurs near top dead center (TDC), and it decreases towards bottom dead center (BDC), where the minimum value of 0.25 MPa is observed. This behavior arises because the ringliner normal force is primarily governed by the instantaneous pressure differential and the ring back pressure, both of which reach their maximum near TDC and decrease to their minimum near BDC. Meanwhile, under mixed-contact conditions, part of the applied load is

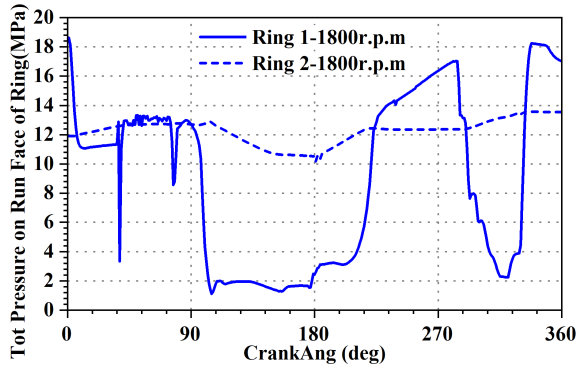

(a) Total contact pressure on the ring running face

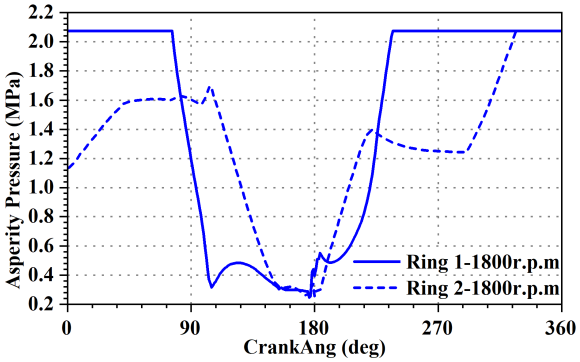

(b) Asperity contact pressure on the ring running face

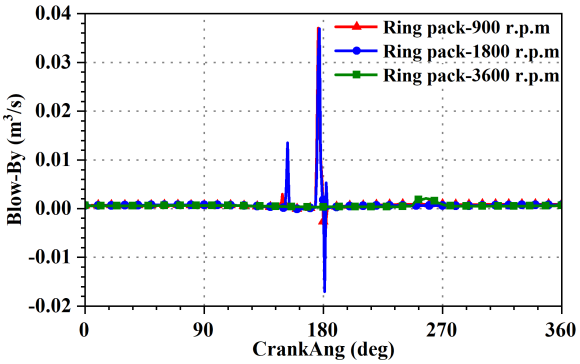

(c) Effect of engine speed on blow-by

Fig. 7. Frictional dynamic characteristics of the piston ring system

carried by the non-asperity contact component; therefore, the roughcontact pressure does not vary linearly with the total contact pressure. During the steady wear stage, the presence of a relatively stable transfer film, together with filler transfer and asperity-flattening effects, further suppresses extreme asperity overloading and helps mitigate pressure spikes, thereby maintaining the system in a stable mixed-contact regime.

Fig. 7c show that the ring-pack blow-by is relatively large near bottom dead center. This is because the pressure differential between the two chambers is smallest at that location and the gas more readily expands and flows, which increases blow-by; blow-by is smaller at other crank angles. Within the rotational speed range of 900 to 1800r/min, the influence of speed on the cycle-averaged blow-by is not significant. However, when the rotational speed is increased to 3600r/min, the average blow-by decreases from 0.0016 m^3/s to 0.0005 m^3/s, corresponding to a reduction of approximately 68.8%. Therefore, a moderate increase in speed can help reduce instantaneous blow-by and inter-chamber gas exchange; however, higher speeds raise the ring wear rate and shorten ring life, so a trade-off between sealing efficiency and service life is necessary.

3.2. Wear of piston rings

Fig. 8 shows the wear characteristics of the rings. Fig. 8a presents the radial total wear depth profile of the running surface; Fig. 8b gives the radial depth wear rates at different rotational speeds; and Fig. 8c shows the radial wear depth as a function of accumulated operating time.

Fig. 8a indicates that, under the rated condition (1800r/min) after 100 hours of cumulative operation, the maximum radial wear depths of the top ring and the second ring are both located in the mid-axial region, and are 0.121 mm and 0.114 mm, respectively. For all investigated cases, the maximum radial wear depth consistently appears in the mid-axial region of the running surface. This behavior can be interpreted based on the Archard wear formulation, in which the local wear rate is proportional to the product of the local normal contact pressure and sliding velocity. Consequently, the axial location with the highest time-averaged pressure-velocity (PV) level will accumulate the greatest wear. Due to the barrel-shaped ring profile and slight ring tilting during operation, the mid-axial region maintains more continuous and stable contact with the liner, resulting in higher time-averaged contact pressure and longer effective sliding duration. In contrast, the edge regions experience partial unloading and intermittent contact, which reduces the local PV level and limits wear accumulation. In addition, thermal effects caused by the temperature gradient further enhance this nonuniform distribution. The mid-axial region operates under relatively higher thermal loading, which can locally reduce the effective hardness of the PTFE composite and slightly increase the wear coefficient. These effects intensify wear in this region. As shown in Fig. 8b, the radial depth wear rate increases significantly with increasing rotational speed. When the speed is increased from 1800r/min to 3600r/min, the depth wear rates of Ring 1 and Ring 2 increase by 121.5% and 116.5%, respectively. Moreover, the rate of wear growth accelerates as rotational speed continues to increase. Fig. 8c demonstrates

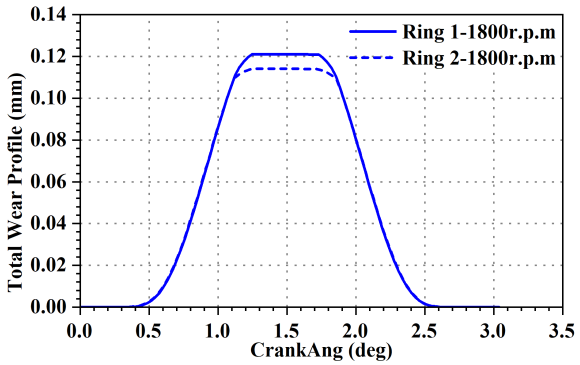

(a) Total wear of the ring running surface profile (100 h)

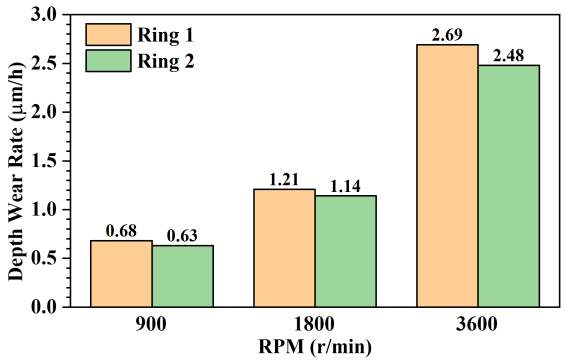

(b) Radial wear rate of the rings at different engine speeds

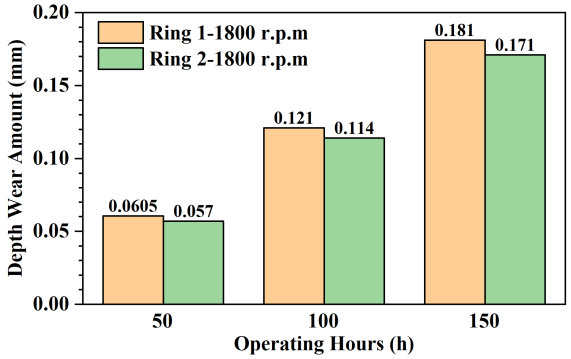

(c) Variation of ring wear depth with operating time

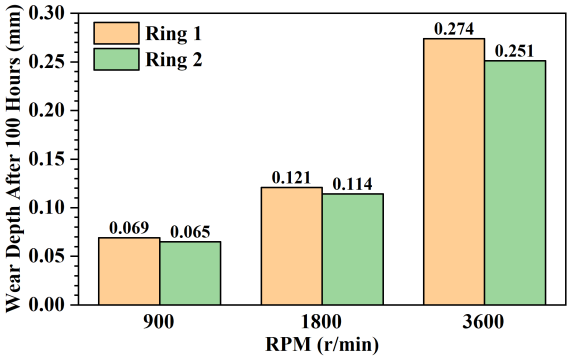

(d) wear depths after working for 100 hours

Fig. 8. Wear characteristics of the rings

Table 2. Summary of key simulation results at different rotational speeds

Parameter \ r.p.m	900	1800	3600	Δ% (900 to 1600)
Ring 1				
Max friction force (N)	358.5	392.3	387.1	+8.0%
Avg friction force (N)	143.4	147.9	142.1	-0.9%
Max power loss (W)	683.3	1360	3068.2	+349.0%
Avg power loss (W)	216.9	470.2	1055.6	+386.7%
Depth wear rate (μm/h)	0.68	1.21	2.69	+295.6%
Ring 2				
Max friction force (N)	165.1	163.7	77.2	-53.2%
Avg friction force (N)	91.6	94.8	89.9	-1.9%
Max power loss (W)	407	590	738.1	+81.3%
Avg power loss (W)	196.1	309.3	293.7	+49.8%
Depth wear rate (μm/h)	0.63	1.14	2.48	+293.7%
Ring back				
Avg blow-by (m^3/s)	0.0016	0.00125	0.0005	−68.8%

that, as operating time increases, the wear of both rings grows and the difference between them widens, indicating that the top ring operates under more severe conditions and is more prone to premature failure.

Fig. 8d presents the wear depths of the rings after 100 hours of continuous operation at different rotational speeds. When the rotational speed increases from 900 to 3600r/min, the wear depths of Ring 1 and Ring 2 increase by 297% and 286%, respectively, demonstrating a nonlinear accelerated increase in wear with rising rotational speed.

Table 2. Summary of key friction, wear, and sealing performance metrics of the piston ring system at different rotational speeds. Relative percentage changes from 900 r/ min to 3600r/ min are provided to enable direct quan-

titative comparison of speed effects and to highlight the trade-off between frictional losses, wear severity, and sealing performance.

4. Conclusions

a) Under the rated condition (1800r/min): The instantaneous friction force peaks for the top ring and the second ring occur at top dead center, reaching 392.3 N and 163.7 N, respectively. The peaks of frictional power loss are 1360 W and 590 W, concentrated in the first half of the expansion stroke after top dead center. The total contact pressure of the top ring fluctuates widely (1.3 MPa to 18.9 MPa), whereas that of the second ring remains more stable (10.25 MPa to 13.55 MPa). The asperity contact pressure of both rings reaches its maximum at top dead center (2.075 MPa) and its minimum at bottom dead center (0.25 MPa). The blow by of the ring pack increases sharply near bottom dead center. The top ring exhibits a higher depth wear rate than the second ring (0.121 mm vs. 0.114 mm after 100 hours of operation).

b) The influence of rotational speed on the cycle averaged friction force is limited (varying within $\pm 2\%$ over the range of 900 to 3600r/min). However, the frictional power loss increases significantly with speed: the cycle averaged power loss of the top ring rises by approximately 386.7%, and that of the second ring by about 49.8%.

c) The radial depth wear rate increases markedly with rotational speed. From 900r/min to 3600r/min, the wear rate of the top ring increases by about 295.6%, and that of the second ring by about 293.7%. The maximum wear consistently appears in the mid axial region, which is attributed to the highest time averaged pressure velocity (PV) level and relatively high local thermal load in that zone.

d) Conversely, sealing performance improves at higher speeds. Owing to enhanced dynamic sealing and a shorter effective leakage time per cycle, the cycle averaged blow by decreases by approximately 68.8% when the speed increases from 900r/min to 3600r/min. These results reveal a clear trade off between improved sealing capability and accelerated wear at elevated rotational speeds.

In summary, the present findings provide a valuable reference for the material selection, geometric optimization, operational condition assessment, and balancing of sealing performance against service life of oil-free piston rings in double-acting Stirling engines operating within the $900 - 3600$r/min range. Although the numerical values reported here are specific to the studied system configuration, the coupled modeling framework integrating multibody dynamics, the Greenwood-Tripp rough-contact model, and the Archard wear theory is generally applicable to other reciprocating machinery employing self-lubricating composite rings. Furthermore, the universal trends identified in this study-such as pressure-dominated friction near top dead center, nonlinear growth of power loss with speed, and the trade-off between sealing enhancement and wear acceleration-can support the design optimization of similar high-pressure oil-free sealing systems.

5. Acknowledgements

This work was supported by National Natural Science Foundation of China (Grant Nos.51606116, 52476212) and Project of Shanghai Municipal Science and Technology Commission (Grant No. 19195810800).

nomenclature

Acronyms

α	linear thermal expansion coefficient of the ring material ($^\circ C^{-1}$)
$\tilde{\beta}$	asperity mean summit radius (μm)
ΔA	wear area (m^2)
Δh	the increment of wear depth (mm)
Δt	time interval (s)
η_s	Number of summits in the nominal area $A(-)$
σ	tensile stress (MPa)
σ_s	R.M.S surface roughness (μm)
$\underline{\varepsilon}$	radial tensile elastic deformation of the ring caused by the temperature (mm)
A_e	size of the straight cut opening (mm)
d	inner diameter of the ring (mm)
E^*	composite elastic modulus (MPa)
$F_{5/2}$	the form function (-)
F_{bending}	bending force caused by the interaction between the thrust and antithrust sides (N)
$F_{\text{contact, rad}}$	contact force between the ring running surface and the cylinder liner (N)
$F_{\text{contact, ax}}$	contact force between the ring and the groove (N)
$F_{\text{fric,ax}}$	friction force between the cylinder wall and ring running surface (N)
$F_{\text{gas ,ax}}$	gas force (N)
$F_{\text{inertia, ax}}$	inertia force (N)
F_d	the sliding frictional force (N)
F_f	static friction force of the piston ring in the static sealing state (N)
H	Brinell hardness of the softer contacting material (N/mm^2)
h	ring's axial thickness (mm)
h_{wear}	wear depth (mm)
H_s	nominal clearance between the contacting surfaces (mm)
K	the dimensionless wear coefficient (-)
L	contact area between the ring and the liner (mm^2)
P	local normal pressure acting on the wear area (MPa)
p	ring back-pressure (MPa)
P_1	pressure of the sealing medium (MPa)
p_t	the pressure as a function of time (MPa)
Q_1	radial wear volume (mm^3)
R	ring's mean radius during operation (mm)
R_0	ring's mean radius at ambient (room) temperature (mm)
S	sliding distance (mm)
t	ring's radial width (mm)
T_0	initial temperature ($^\circ$C)
T_1	operating temperature ($^\circ$C)
v	Poisson's ratio (-)
v_r	relative sliding velocity (mm/s)
D	outer diameter of the ring (mm)
E	Young's modulus of the piston ring material (MPa)

F	normal load applied to the contact surfaces (N)
Ks	wear modulus (mm^3/Nm)
V	wear volume (mm^3)

References

[1] D. G. Thombare and S. K. Verma, (2008) *"Technological development in the Stirling cycle engines"* **Renewable and Sustainable Energy Reviews *12***(1): 1–38. DOI: 10.1016/j.rser.2006.07.001.

[2] J. Zou. *Stirling Engine*. 1st ed. Changsha: Hunan University Press, 1985, Chapter 3.

[3] H. Hachem, R. Gheith, F. Aloui, and S. Ben Nasrallah, (2018) *"Technological challenges and optimization efforts of the Stirling machine: A review"* **Energy Conversion and Management *171***: 1365–1387. DOI: 10.1016/j.enconman.2018.06.042.

[4] S. Zare and A. Tavakolpour-Saleh, (2019) *"Free piston Stirling engines: A review"* **International Journal of Energy Research *44***(7): 5039–5070. DOI: 10.1002/er.4533.

[5] M. H. Briggs. "Improving power density of free-piston stirling engines". In: *14th International Energy Conversion Engineering Conference*. 2016, 5016. DOI: 10.2514/6.2016-5016.

[6] G. Walker. *Stirling engines*. Oxford: Oxford University Press, 1980, Chapter 3.

[7] B. Brushan and D. F. Wilcock, (1982) *"Wear behavior of polymeric compositions in dry reciprocating sliding"* **Wear *75***(1): 41–70. DOI: 10.1016/0043-1648(82)90139-9.

[8] Y. Diao and A. Wei, (2004) *"Friction and Wear Analysis of Self-lubrication Piston Ring"* **Lubrication Engineering *29***(05): 103–106.

[9] J. Ye, D. Burris, and T. Xie, (2016) *"A Review of Transfer Films and Their Role in Ultra-Low-Wear Sliding of Polymers"* **Lubricants *4***(1): DOI: 10.3390/lubricants4010004.

[10] T. W. Scharf and S. V. Prasad, (2013) *"Solid lubricants: a review"* **Journal of Materials Science *48***(2): 511–531. DOI: 10.1007/s10853-012-7038-2.

[11] H. Guo, J. Zhao, and X. Sun, (1990) *"A Study on the Wear Mechnism of Filled Oilless Sliding Materials"* **Journal of Beijing University of Aeronautics and Astronautics** (04): 32–39. DOI: 10.13700/j.bh.1001-5965.1990.04.006.

[12] J. Wang, X. Huang, W. Wang, H. Han, H. Duan, S. Yu, and M. Zhu, (2022) *"Tribological behavior and film-forming mechanism of a polytetrafluoroethylene/polyester fabric composite"* **Industrial Lubrication and Tribology *74***(1): 65–72. DOI: 10.1108/ILT-07-2021-0246.

[13] R. Huang, S. Ma, M. Zhang, J. Yang, D. Wang, L. Zhang, and J. Xu, (2019) *"Wear Evolution of the Glass Fiber-Reinforced PTFE under Dry Sliding and Elevated Temperature"* **Materials (Basel) *12***(7): 1082. DOI: 10.3390/ma12071082.

[14] H. C. Meng and K. C. Ludema, (1995) *"Wear models and predictive equations: their form and content"* **Wear *181-183***: 443–457. DOI: 10.1016/0043-1648(95)90158-2.

[15] S. K. Rhee, (1970) *"Wear equation for polymers sliding against metal surfaces"* **Wear *16***(6): 431–445. DOI: 10.1016/0043-1648(70)90170-5.

[16] S. Xu, H. Li, and Z. Su, (2019) *"Fitting of Wear Formula of Filled PTFE Based on Finite Element Analysis Method"* **Lubrication Engineering *44***(09): 142–146.

[17] V. Singh and A. Kumar, (2024) *"A Systematic and Comprehensive Review on 2-D and 3-D Numerical Modelling of Stirling Engine"* **Archives of Computational Methods in Engineering *31***(6): 3255–3266. DOI: 10.1007/s11831-024-10080-z.

[18] G. Gu, D. Jin, and T. Yan, (2000) *"Study on the Stirling Engine Dynamic Characteristics"* **Transactions of CSICE** (03): 305–307. DOI: 10.16236/j.cnki.nrjxb.2000.03.018.

[19] H.-S. Yang, C.-H. Cheng, and S.-T. Huang, (2018) *"A complete model for dynamic simulation of a 1-kW class beta-type Stirling engine with rhombic-drive mechanism"* **Energy *161***: 892–906. DOI: 10.1016/j.energy.2018.07.159.

[20] C.-H. Cheng and Y.-J. Yu, (2012) *"Combining dynamic and thermodynamic models for dynamic simulation of a beta-type Stirling engine with rhombic-drive mechanism"* **Renewable Energy *37***(1): 161–173. DOI: 10.1016/j.renene.2011.06.013.

[21] Y. Q. Lian, Q. C. Xu, and D. K. Ren, (2012) *"Life Prediction of the Oil-Free Piston Rings in the Air-Powered Swashplate Engine"* **Advanced Materials Research *538-541***: 3008–3011. DOI: 10.4028/www.scientific.net/AMR.538-541.3008.

[22] S. Hou, L. Zhang, and X. Zhang. "Friction analysis for piston ring of seal device in the stirling engine". In: *2nd International Conference on Electronic & Mechanical Engineering and Information Technology*. Atlantis Press. 2012, 987–991. DOI: 10.2991/emeit.2012.214.

[23] D. Y. Yang, H. Xie, and J. Gong, (2013) *"The Analysis of the Influencing Factors about Friction and Wear Characteristics of the Piston Ring in Stirling Engine"* **Advanced Materials Research *690-693***: 2003–2007. DOI: 10.4028/www.scientific.net/AMR.690-693.2003.

[24] D. Xin, J. Feng, Y. Xu, and X. Peng, (2010) *"Investigation of Pressure Distribution and Frictional Heat on Self-Lubricated Piston Rings in Reciprocating Compressors"* **Compressor Technology *48***(06): 8–12. DOI: 10.16051/j.cnki.ysjjs.2010.06.010.

[25] J. Zen, Y. Peng, X. Dai, and R. Xiao, (2015) *"Numerical Calculation of Flow esistance Characteristics of Double-acting Stirling Engine Piston Sealing"* **Lubrication Engineering *40***(06): 95–99.

[26] J. F. Archard, (1953) *"Contact and Rubbing of Flat Surfaces"* **Journal of Applied Physics *24***(8): 981–988. DOI: 10.1063/1.1721448.

[27] M. Hanief and M. S. Charoo, (2021) *"Archard's wear law revisited to measure accurate wear coefficient considering actual sliding velocity"* **Materials Today: Proceedings *47***: 5598–5600. DOI: 10.1016/j.matpr.2021.03.475.

[28] M. Varenberg, (2022) *"Adjusting for Running-in: Extension of the Archard Wear Equation"* **Tribology Letters *70***(2): DOI: 10.1007/s11249-022-01602-6.

[29] Y. Ding, P. Li, C. Xing, X. Kang, Y. Lv, X. Du, X. Gao, and Y. Li, (2025) *"Lifespan prediction of the piston ring set of oil-free reciprocating compressors coupled with pressure distribution variation"* **Engineering Failure Analysis *171***: 109317. DOI: 10.1016/j.engfailanal.2025.109317.

[30] N. Békési, K. Váradi, and D. Felhős, (2011) *"Wear Simulation of a Reciprocating Seal"* **Journal of Tribology *133***(3): DOI: 10.1115/1.4004301.

[31] W. Cao, Z. Chang, A. Zhou, X. Dou, G. Gao, and J. Gong, (2022) *"Investigation into the Influence of Parallel Offset Wear on Stirling Engine Piston Rod Oil-Free Lubrication Seal"* **Machines *10***(5): 350. DOI: 10.3390/machines10050350.

[32] F. Razavirad, N. Kristensen, J. de Claville Christiansen, and M. M. B. Bak, (2025) *"A computational study on wear behavior in piston ring-cylinder liner assemblies"* **Proceedings of the Institution of Mechanical Engineers, Part J: Journal of Engineering Tribology *240***(1): 119–138. DOI: 10.1177/13506501251337966.

[33] M. Ahmed Ali, H. Xianjun, R. Turkson, and M. Ezzat, (2015) *"An analytical study of tribological parameters between piston ring and cylinder liner in internal combustion engines"* **Proceedings of the Institution of Mechanical Engineers, Part K: Journal of Multi-body Dynamics *230***(4): 329–349. DOI: 10.1177/1464419315605922.

[34] K. Mahmoud, O. Knaus, T. Parikyan, and M. Patete. "Three dimensional ring dynamics modeling approach for analyzing lubrication, friction and wear of piston ring-pack". In: *Internal Combustion Engine Division Fall Technical Conference*. ***58325***. American Society of Mechanical Engineers. 2017, V002T06A013. DOI: 10.1115/ICEF2017-3586.

[35] K. G. Mahmoud, O. Knaus, T. Parikyan, G. Offner, and S. Sklepic, (2018) *"An integrated model for the performance of piston ring pack in internal combustion engines"* **Proceedings of the Institution of Mechanical Engineers, Part K: Journal of Multi-body Dynamics *232***(3): 371–384. DOI: 10.1177/1464419317736676.

[36] Y. Zhu, (2008) *"Design and calculation on work clearance and relative interference amount of non-backpressure piston rings"* **Journal of Hebei University of Science Technology *29***(1): 53–56.

[37] Y. Zhu, (2006) *"Research on design of integral non-backpressure piston rings in compressors"* **Lubrication Engineering *31***(12): 106–107.

[38] N. P. Suh, (1973) *"The delamination theory of wear"* **Wear *25***(1): 111–124. DOI: 10.1016/0043-1648(73)90125-7.

[39] C. Delprete, E. Selmani, and A. Bisha, (2019) *"Gas escape to crankcase: impact of system parameters on sealing behavior of a piston cylinder ring pack"* **International Journal of Energy and Environmental Engineering *10***(2): 207–220. DOI: 10.1007/s40095-019-0296-x.

[40] H. X. Xu, W. Song, W. B. Ying, X. N. Cheng, and X. H. Yuan, (2007) *"Mechanical properties of PTFE compositesrein forced by glass fiber and graphite"* **Journal of Jiangsu University(Natural Science Edition) *37***(05): 401–404.

[41] B. Menacer, S. Narayan, V. Tuninetti, T. Khatir, A. Oñate, L. Osorio, S. Abubakar, J. Samuel, I. Grujic, N. Stojanovic, and M. U. Kaisan, (2024) *"Impact of Influence of Piston Design Parameters on the Hydrodynamic Characteristics of Internal Combustion Engines—A Numerical Study"* **Lubricants *12***(12): 427. DOI: 10.3390/lubricants12120427.

[42] B. Bhushan, (1984) *"Analysis of the Real Area of Contact Between a Polymeric Magnetic Medium and a Rigid Surface"* **Journal of Tribology *106***(1): 26–34. DOI: 10.1115/1.3260862.

[43] H. Li, R. Yang, and Z. Su, (2023) *"Effect of different rigid reinforcing fillers on properties of PTFE"* **China Plastics *37***(08): 13–19. DOI: 10.19491/j.issn.1001-9278.2023.08.003.

[44] Q. Yao, Y. Wen, J. Yu, and R. Zhang, (2012) *"Research on Strueture Design of Elastic Composite Cylindrical Roller Bearing"* **China Mechanical Engineering *23***(24): 2899–2902.

[45] S. Zhang, H. Song, S. Sandfeld, X. Liu, and Y. G. Wei, (2019) *"Discrete Greenwood–Williamson Modeling of Rough Surface Contact Accounting for Three-Dimensional Sinusoidal Asperities and Asperity Interaction"* **Journal of Tribology *141***(12): DOI: 10.1115/1.4044635.

[46] J. A. Greenwood and J. H. Tripp, (1967) *"The Elastic Contact of Rough Spheres"* **Journal of Applied Mechanics *34***(1): 153–159. DOI: 10.1115/1.3607616.

[47] D. Xin, J. Feng, L. Ding, D. Yang, and X. Peng, (2012) *"Experimental investigation of pressure distribution between the piston rings and its formation in reciprocating compressors"* **Proceedings of the Institution of Mechanical Engineers, Part C: Journal of Mechanical Engineering Science *226***(11): 2701–2712. DOI: 10.1177/0954406212438151.